Dissimilar Material Joints With and Without Free-edge Stress Singularities: Part II. An Integrated Numerical Analysis

by L.R. Xu and S. Sengupta

ABSTRACT—Numerical investigations were conducted on plane and axisymmetric convex joints of polycarbonate–aluminum and poly(methyl methacrylate)–aluminum interfaces to gain a better understanding of the stress state along the interface and also to aid an experimental study conducted on the same issue. Two-dimensional plane–stress investigations of convex joints revealed the successful elimination of the free-edge stress singularities along the specimen width although stress singularities, along the thickness direction, persisted. A convex axisymmetric design, with the same material combination and joining angles, proves to be a better design in order to achieve an overall elimination of free-edge stress singularities of dissimilar materials and structures.

KEY WORDS—Bonding, dissimilar materials, finite element, stress singularities, axisymmetric

Introduction

Researchers have shown that the presence of free-edge stress singularities in bi-material corners or edges leads to erroneous results in interfacial strength measurements.[1,2] To address this issue, a convex plane-joint was developed to remove the free-edge stress singularities. In Part I of this investigation,[3] plane-joints of polycarbonate–aluminum and poly(methyl methacrylate)–aluminum (PMMA–aluminum) interfaces were tested using an *in situ* photoelasticity technique. Experimental results showed that failure load values of the same interface with different edge shapes were quite different. In order to understand the insight into the mechanics, a numerical investigation will be very necessary since the photoelasticity method mainly provided information of a two-dimensional stress state. Indeed, in modern experimental studies, integrated numerical simulations not only validate experimental results, but also reduce possible errors inherent in experimental setups.

In this investigation, a two-dimensional finite-element analysis will be conducted to verify and compare stress changes in the convex plane-joints to experimental findings. However, three-dimensional finite element analysis shows that the stress singularity along the thickness direction still exists. So, a convex axisymmetric joint will be proposed to provide reasonable interfacial strength measurements.

Finite-element Modeling

Elastic finite-element analysis of the baseline and the proposed convex metal–polymer (aluminum–polycarbonate) joint specimen was carried out employing a commercial software ANSYS. The dimensions of the baseline specimen (straight edge; see Fig. 1(a)) were: length $L = 254$ mm; half-width $W = 19.05$ mm; thickness $2T = 6.35$ mm for thin specimens and 9.2 mm for thick specimens. In this investigation, four different joint types, with the same bi-material combination and equal bonding area, were subjected to the same in-plane tension load, as shown in Fig. 1. One was the traditional butt-joint specimen with straight free-edges (Fig. 1(a)). It was expected that severe stress singularities would be observed at the free-edge in this baseline specimen. The second specimen had convex edges with proposed interfacial joint angles, as seen in Fig. 1(b). It should be mentioned here that our proposed new joint design reduced the material volume by at least 15% around the interfacial joint area. Greater reduction in total material volume would be attained if the area away from the interface is taken into account. The third specimen was a straight cylinder with free edges as shown in Fig. 1(c). This was used to illustrate the advantage of the convex edges of Fig. 1(d) over the straight edges of Fig. 1(c). The fourth specimen, as illustrated in Fig. 1(d), was an axisymmetric design with convex edges. Equating the interfacial bonding area of Fig. 1(d) to that of the three-dimensional non-axisymmetric specimen (Fig. 1(b)) yielded the radius of the axisymmetric specimen.

A detailed illustration of the mesh used for the convex plane-joint is shown in Fig. 2, where the gradual change in element size, from coarsely to finely meshed regions, may be noticed. Taking advantage of symmetry, only half of the specimen was modeled. The transition from the straight edge to the curved edge at the interface corner was achieved by means of a circular arc of radius $R = \{t/[1 - \sin(\theta)]\}$, where θ is the joining angle and t is the convex extension distance, as illustrated in Fig. 2(a). Roller boundary conditions were applied along the mid-plane of the specimen, i.e., at $x = W$. The finite-element mesh consisted of PLANE 42 elements (two-dimensional four-noded element) and finer subdivisions were used in regions where the stress gradient was expected to be high, such as the interface corner and the entire length of the interface. For the straight-edged specimens, the element

L.R. Xu (SEM Member; l.roy.xu@vanderbilt.edu) is an Assistant Professor and S. Sengupta is a Graduate Research Assistant, Department of Civil and Environmental Engineering, 2301 Vanderbilt Place, Vanderbilt University, Nashville, TN 37235, USA.

Original manuscript submitted: December 30, 2003.
Final manuscript received: September 14, 2004.
DOI: 10.1177/0014485104049397

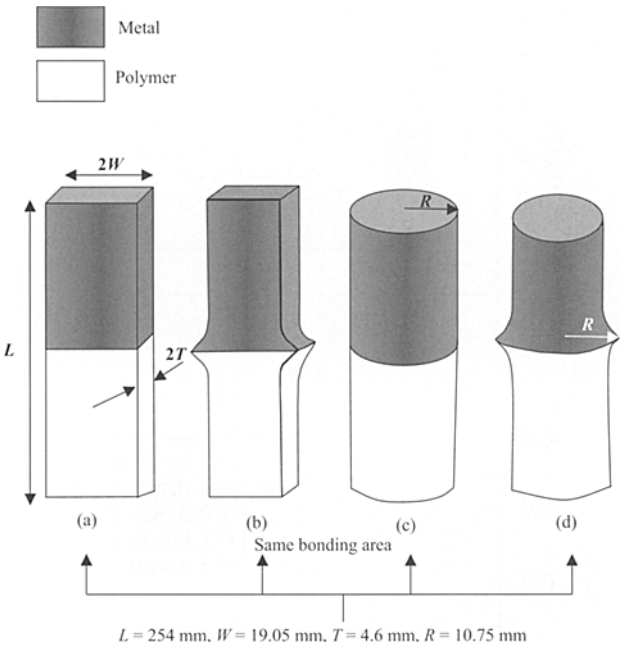

Fig. 1—Schematic diagrams of aluminum–polycarbonate joint specimens with (a) straight edges (baseline), (b) shaped edges with least stress singularities, (c) axisymmetric design of straight-edge specimen, and (d) axisymmetric design of shaped edge specimen

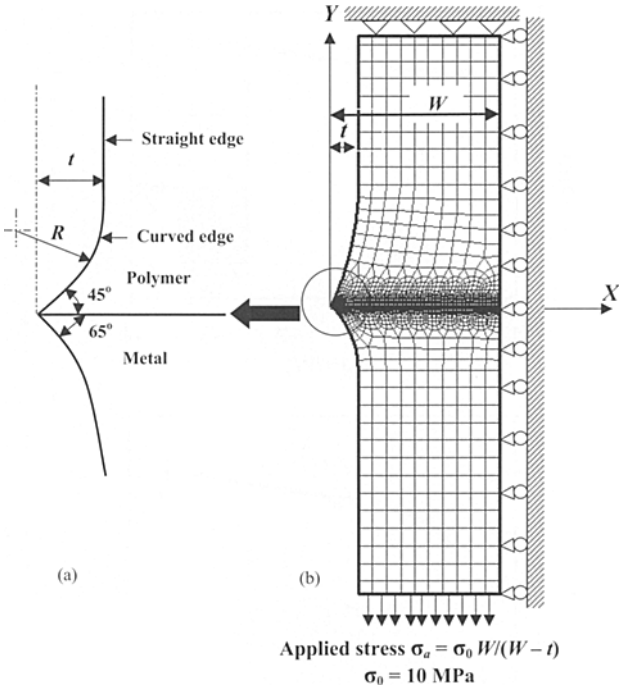

Fig. 2—(a) Illustration of a proposed convex joint of metal and polymer interface. (b) Finite-element mesh and boundary conditions of the new joint subjected to in-plane tensile load. Note that the applied stress at the specimen end is a function of t such that the average tensile stress at the interface is always 10 MPa. W is the half-width of the specimen

length ranged from a maximum of 0.1 W to a minimum of 0.000407 W. While the maximum element edge length was retained in meshing the convex specimens, the smallest element length was changed to 0.000794 W in order to utilize the same meshing pattern for both the shaped and baseline (straight-edge) specimens. The finite-element model was loaded by applying tension to the edge parallel to the x-axis at $y = -127$ mm. The edge at $y = 127$ mm was specified with zero displacement boundary conditions in the y-direction. Assuming that the same total load at the same interface area was transferred to both baseline and shaped specimens, the stress applied to the shaped specimen was obtained by multiplying the stress σ_0 (stress applied to the baseline specimen) by a factor of $W/(W-t)$. The stiffness properties for aluminum were chosen as $E = 71$ GPa, $\nu = 0.33$, and for polycarbonate, $E = 2.4$ GPa, $\nu = 0.34$.

A similar approach was taken for the three-dimensional analysis of the same convex plane-joint (Fig. 1(b)) except that the two-dimensional mesh was extruded in the Z-direction to achieve the thickness of the specimen. While two-dimensional plane stress elements (PLANE42) and two-dimensional axisymmetric elements (PLANE42) were used for modeling, the two-dimensional plane stress and axisymmetric models, respectively, iso-parametric quadrilateral 20-node SOLID95 elements, were used to construct the three-dimensional model. Taking advantage of symmetry, a quarter of the model was used in three-dimensional analysis. Submodeling was utilized in the three-dimensional design to ensure a fine mesh in the close vicinity of the bimaterial interface.

Results and Discussion

Influence of Geometrical Shapes and Material Properties

In order to validate our numerical analysis results, we compared the stress singularity order, λ, obtained from the finite-element analysis and from Bogy's formula.[3,4] The approach adopted here is similar to that described by Munz and Yang.[5] An aluminum–polycarbonate interface with joining angles of 90°–90° was considered, and the results are illustrated in Fig. 3. On applying 10 MPa stress in the Y-direction, the interfacial normal stress and shear stresses were plotted as functions of the ratio r/W. Here, r is the distance from the interface corner and W is the half-width of the specimen. According to the defining relation between λ and the stresses at the interface,[3] the slopes of these respective plots should yield the value of λ. From Fig. 3, it is seen that the slope as obtained from the interfacial normal stress plot is equal to 0.223 and the slope of the interfacial shear stress plot is 0.216. The analytical value of λ based on Bogy's formula is 0.225 for these specific materials and angle joints. These three values are quite close, and hence we shall use the same tool and procedure to analyze the proposed convex joints.

The main parameters that have been varied in our finite-element analysis are (i) convex extension distance t, (ii) joining angles, and (iii) elastic constants of the constituent materials. The influence of the geometrical parameters, on the stress distribution at the interface, is illustrated in Figs. 4 and 5. Four cases have been examined for $t = 0$ (straight-edge or

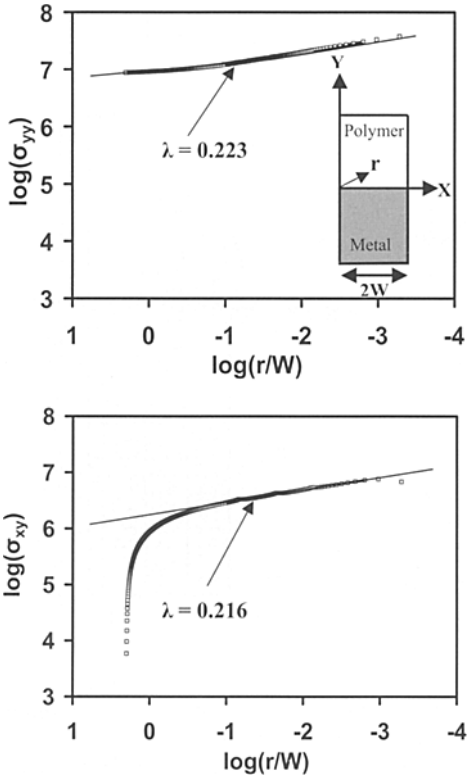

Fig. 3—Comparison of the stress singularity order λ obtained from the finite-element analysis and Bogy's formula for an Al–PC joint with straight edges. (a) Finite-element interfacial normal stress distribution close to free edge and fitted λ value. (b) Finite-element interfacial shear stress distribution close to free edge and fitted λ value. Theoretical λ = 0.225.

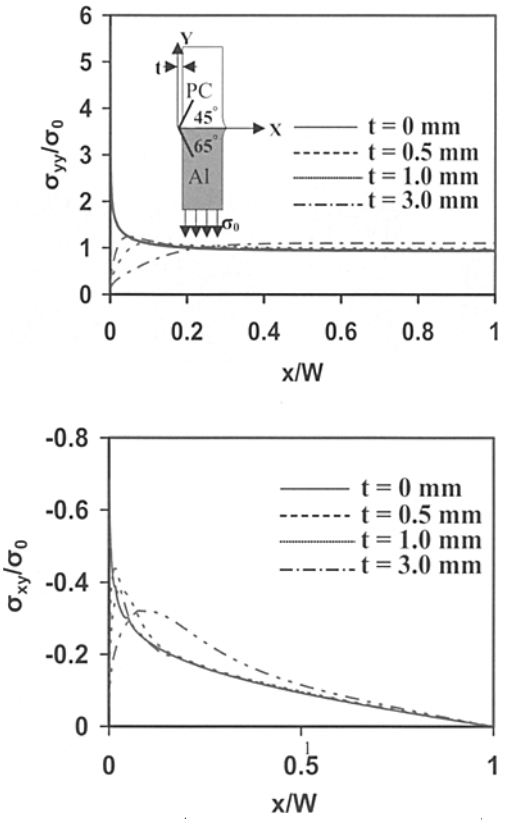

Fig. 4—Variations of (a) interfacial normal stress and (b) interfacial shear stress with different extension distances (fixed joint angles θ_1 (for polycarbonate) = 45°; θ_2 (for aluminum) = 65°). If t = 0 (straight edge), stresses are singular at the free edges

baseline specimens), 0.5, 1.0 and 3.0 mm. For zero extension distance, i.e., straight-edge specimens, a prominent stress singularity is seen at the bi-material corner. However, for increasing extension distances, the interfacial normal stress and shear stress have finite values at the interface corner, and their respective distributions are seen to smoothen out over the interface to uniform values. From this analysis, we find that the free-edge stress singularity is successfully removed and the convex extension distance t mainly affects local stress distributions close to free-edges. Since stress singularity directly contributes to free-edge delamination or debonding, this results in a corresponding increase of the load transfer capability of the new joint as long as we use the specific convex joint. However, convex specimens may not be accurately machined. So a natural question arises, should we use the exact interfacial joint 45°–65° angle combination only? Figure 5 is significant in that while only the 45° angle of the polycarbonate part was retained and the joint angle of the aluminum part was varied from 45° to 90°, the stress singularity was still effectively removed. This example, along with other similar numerical case studies, essentially points to the fact that as long as the sum of two joint angles is less than 180° and each joint angle is less than 90°, the stress singularities will be reduced. In other words, stress singularity is successfully removed for the 45°–65° angle combination in theory but, in reality, for a slight deviation from this combination, the stress singularity would be reduced if not removed absolutely. Our next question therefore is, would this statement

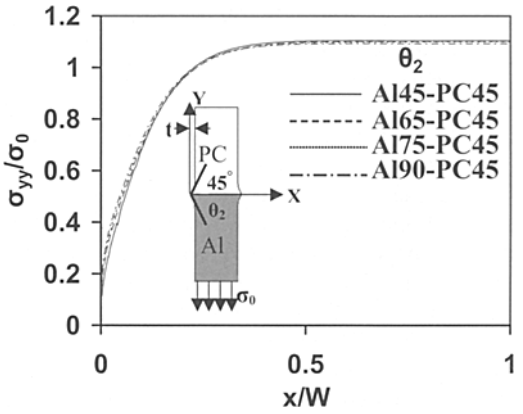

Fig. 5—Variation of normalized interfacial normal stress with the joint angle of aluminum (fixing the joint angle of PC at 45°, t = 3 mm)

hold true for most of the material combinations as shown in Fig. 3 of Part I[3] of this investigation?

The influence of material properties on the reduction of stress singularity was examined by retaining the polycarbonate half of the tensile joint specimen and varying Young's modulus of the other material. Four cases were chosen for E_2 = 2.4, 10, 71, and 200 GPa, and the results are illus-

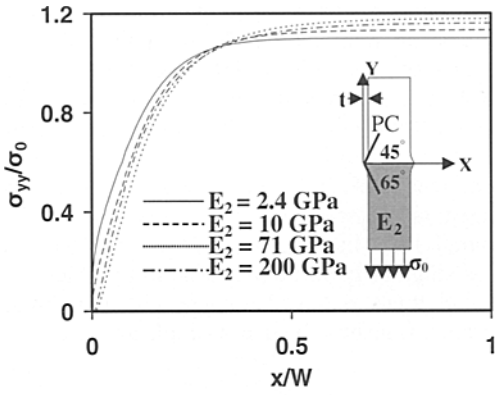

(a)

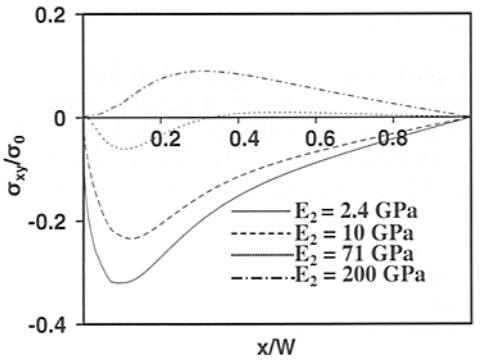

(b)

Fig. 6—(a) Variation of interfacial normal stress and (b) variation of interfacial shear stress with different material properties (keeping polycarbonate the same, t = 3 mm)

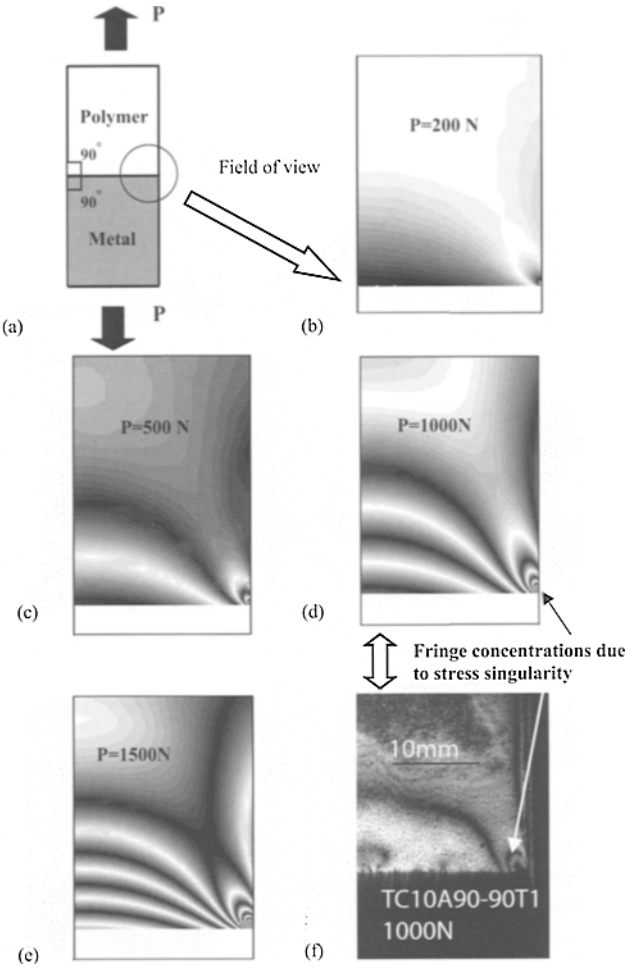

Fig. 7—Development of numerical photoelasticity patterns for load (b) P = 200 N, (c) P = 500 N, (d) P = 1000 N, and (e) P = 1500 N. (f) Experimental photoelasticity pattern for a typical PC/Al joint with straight edges under P = 1000 N

trated in Figs. 6(a) and (b). The results show that while the interfacial normal stress distribution smoothened out over the interface, the interfacial shear stress distribution dipped within 15% of the distance from the joint tip. However, the normal and shear stresses were very near to zero at the interface corner, which has a direct impact on higher load transfer capacity since the interface would be less likely to fail at low load as compared to conventional straight-edged specimens. These numerical results verify the theoretical results shown in Fig. 3 of Part I,[3] and so these convex joints are effective in removing stress singularities for most engineering material combinations.

Comparison of Numerical Analysis with Experimental Results for Plane Joints

We mainly used full-field photoelasticity to make a direct comparison with the finite-element simulation. Figures 7 and 8 bear the most conclusive testimony to the reduction of stress singularity at the interface of dissimilar materials. The photoelastic fringe patterns are contours of the maximum in-plane shear stress according to the classical photoelasticity equation

$$\tau_{max} = (\sigma_1 - \sigma_2)/2 = \frac{N f_\sigma}{2h}, \qquad (1)$$

where σ_1 and σ_2 are in-plane principal stresses, N is the fringe order, f_σ is the stress-fringe constant (7 kN m^{-1} for polycarbonate), and h is the specimen thickness. After the fringe order N was computed at every node using eq (1), a corresponding gray-scale value was calculated by associating a gray-scale value of 255 with full-fringe orders (e.g. 0, 1, 2, etc.) and a value of 0 with half-fringe orders (e.g. 0.5, 1.5, 2.5, etc). Plotting software, Tecplot 9.2, was then used to plot these gray-scale values, and the numerical fringe patterns shown in Figs. 7 and 8 were generated for stress field visualization and comparison with experimental results.

It is rather interesting to note that a clear fringe concentration originates at the interface corner for straight-edged specimens with increasing load, as shown in Fig. 7. This type of fringe concentration is a result of the free-edge stress singularity and is very similar to the fringe concentration caused by a bi-material interfacial crack.[6] We notice that the stress singularity order for Al/PC joints is around –0.2 and can be eliminated, but for interfacial cracks, the stress singularity order is $-0.5 + i\varepsilon$,[7,8,9] and is intrinsic. A direct comparison of the numerical fringe pattern (Fig. 7(d)) and the experimental pattern (Fig. 7(f)) of the specimen subjected to the same applied load of 1000 N verifies the existence of stress singularity at the free edge.

The accumulation of fringes at the bi-material interfacial corner, seen in the straight-edged specimens, completely

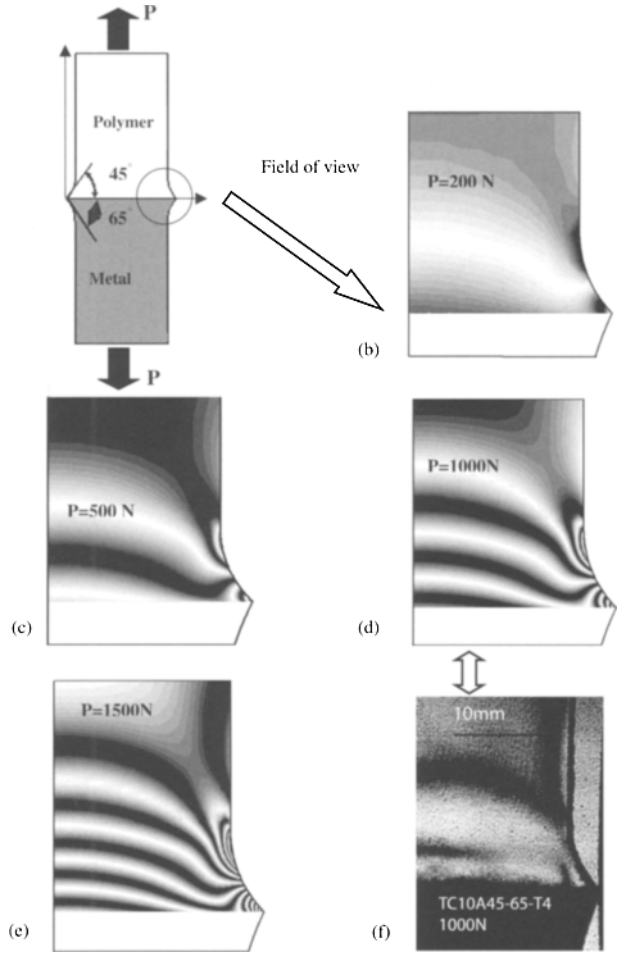

Fig. 8—Development of numerical photoelasticity patterns for load (b) P = 200 N, (c) P = 500 N, (d) P = 1000 N, and (e) P = 1500 N. (f) Experimental photoelasticity pattern for a typical PC/Al joint with shaped edges under P = 1000 N

disappeared in the numerical fringe patterns for the convex specimen, as seen in Fig. 8. The experimental fringe pattern also validates this result, as shown in Fig. 8(f). The highest fringe order actually went up to 23.5 for the straight-edged specimens, whereas the highest fringe order in the shaped specimens under the same applied load (P = 500 N) was only 6.5. This is a clear indication that the stress intensity decreased by several orders in the proposed convex joint. It is noticed that the higher fringe orders signifying larger stress intensity move away from the free-edge towards the polycarbonate curved edge. This stress redistribution is indeed very important in interfacial joint designs since the bonding strength of the interface is generally lower than that of the bulk material (adherend). For example, the tensile strength of bulk polycarbonate is at least 60 MPa, whereas the nominal interfacial tensile strength of PC/Al joints in this investigation is around 5–6 MPa. It may be noticed that the number of fringes in Figs. 8(d) and (f) do not match exactly although the general pattern of stress evolution is distinctly similar. This is because a finite-element simulation assumes ideal conditions unlike the actual *in situ* experiments conducted.

As a result of reduction of the free-edge stress singularity, experiments conducted on PMMA–aluminum and polycarbonate–aluminum convex-shaped specimens showed a marked increase in nominal tensile strengths (ultimate load/interface area) over those of straight-edged specimens.[3] Another interesting experimental phenomenon is the influence of specimen thickness, which has also been considered for polycarbonate–aluminum joints. It was also noticed that thicker specimens (thickness 9 mm) showed less tensile strength increase than thin specimens (thickness 6 mm).[3] This raises an important issue in the convex plane-joint since the free-edge stress singularity still exists around the thickness direction, although it was removed along specimen width direction. This problem can be solved by a simple axisymmetric design.

Axisymmetric Convex Joint for Intrinsic Interfacial Strength Measurements

The convex plane-joint was employed in Part I of this investigation simply because it can be used in direct comparison with *in situ* stress visualization techniques such as photoelasticity. However, careful three-dimensional stress analysis revealed that the removal of free-edge stress singularities is not complete. Figure 9 depicts the distribution of normal and shear stresses of the polycarbonate–aluminum interface along width and thickness directions. The substitution of straight interface ends by convex angles has rendered a smooth stress distribution, without any sign of stress singularity along the width (X-direction). This same conclusion was reached in the two-dimensional finite-element analysis of the same specimen (Fig. 4). We can conclude that Fig. 9(a) could be smoother (with a finer mesh) although the basic nature of the stress distributions would still be the same. The reason a finer mesh could not be used is attributed to the limitation of the finite-element analysis tool used for this purpose. It is not surprising that Fig. 9(b) shows that the stress singularity in the thickness direction still exists. This is because, although the specimen was given a convex shape in the X–Y plane, the stress singularity in the Y–Z plane still persisted due to the existing straight edges. An obvious solution to this problem would be an axisymmetric design where a convex shape is imparted to the entire circumference of the bi-material interface. Indeed, tree mechanics has been an inspiring factor in our research.[10] An axisymmetric convex joint, which is naturally similar to a tree/bamboo shape, will be used to measure the intrinsic interfacial strength.

Figures 10(a) and (b) compare the interfacial stress states in an axisymmetric cylindrical specimen with convex interfacial joints to those in an axisymmetric cylinder with straight edges. Singular stresses are normally expected close to the specimen free-edge, as shown in Fig. 10(a) for the reference purpose of stress state comparison. This impedes us from obtaining an intrinsic interfacial strength. However, Fig. 10(b) clearly shows that stress singularities are eliminated if the axisymmetric design is used in new specimen design. To validate these stress states, more advanced experimental investigations should be conducted[11] since traditional experimental stress analysis techniques, such as photoelasticity, face difficulty in depicting sharp three-dimensional stress change in a small zone close to the specimen free-edge. On the other hand, final tensile strength increase was predicted for the convex axisymmetric specimen over the straight cylindrical joint even before actual experiments were conducted. Definitely, numerical simulation provides clear insight into

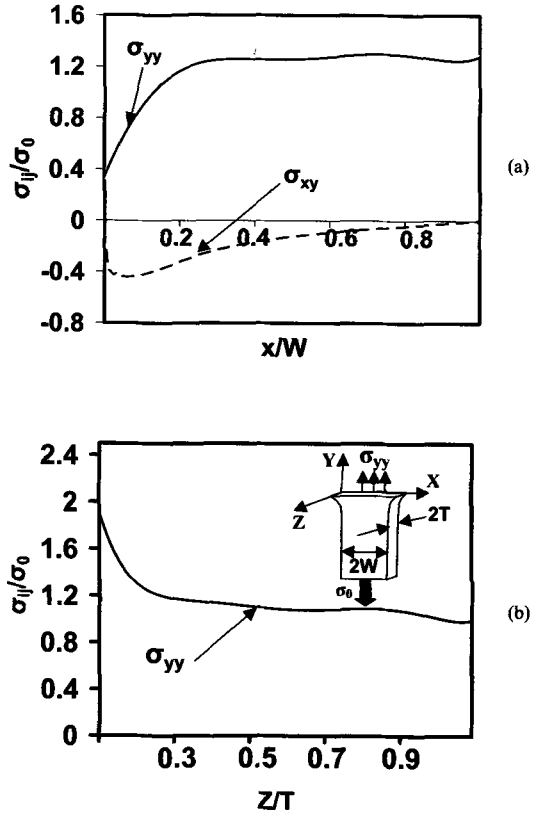

Fig. 9—(a) Variation of interfacial normal stress and shear stress in a three-dimensional finite-element model along width. (b) Variation of interfacial normal stress in a three-dimensional finite-element model along thickness (t = 3 mm)

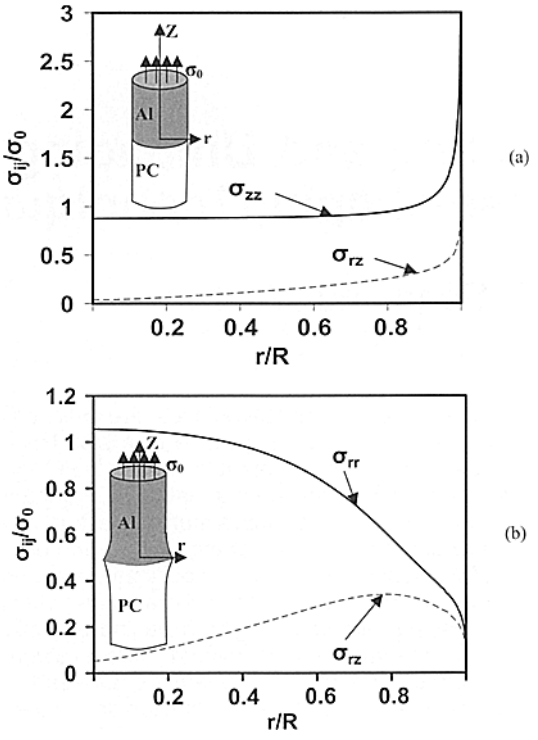

Fig. 10—(a) Variation of interfacial normal stress and shear stress in an unshaped axisymmetric finite-element model. (b) Variation of interfacial normal and shear stress in a shaped axisymmetric finite-element model (t = 3 mm)

mechanics and is very helpful in the investigation of experimental mechanics.

Conclusions

Finite-element analyses on two-dimensional plane-stress, axisymmetric and full three-dimensional specimens were conducted to aid Part I of this investigation. The results are interesting in that the two-dimensional plane-stress specimens were devoid of stress singularities along the specimen width, although the free-edge stresses along the thickness direction were still singular. An axisymmetric design was shown to eliminate stress singularities along the periphery of the bimaterial interface. This should lead to increased load transfer capability of the new joints, and hence the convex axisymmetric specimen is expected to yield intrinsic interfacial tensile strength measurements.

Acknowledgments

LRX gratefully acknowledges the support from the Office of Naval Research Young Investigator Award (N00014-03-1-0505, Dr Roshdy G.S. Barsoum, Program Officer), and the National Science Foundation, Surface Engineering and Materials Design Program (CMS-0409665, Dr Yip-Wah Chung, Program Director).

References

1. Reedy, E.D. and Guess, T.R., "Comparison of Butt Tensile Strength Data With Interface Corner Stress Intensity Factor Prediction," International Journal of Solids and Structures, **30**, *2929–2936 (1993).*

2. Williams, M.L., "Stress Singularities Resulting From Various Boundary Conditions in Angular Corners in Extension," Journal of Applied Mechanics, **19**, *526–528 (1952).*

3. Xu, L.R., Kuai, H., and Sengupta, S., "Dissimilar Material Joints With and Without Free-edge Stress Singularities: Part I. A Biologically Inspired Design," EXPERIMENTAL MECHANICS, **44** *(6), 608–615 (2004).*

4. Bogy, D.B., "Two Edge-bonded Elastic Wedges of Different Materials and Wedge Angles Under Surface Traction," Journal of Applied Mechanics, **38**, *377–386 (1971).*

5. Munz, D. and Yang, Y.Y., "Stress Near the Edge of Bonded Dissimilar Materials Described by Two Stress Intensity Factors," International Journal of Fracture, **60**, *169–177 (1993).*

6. Xu, L.R. and Rosakis, A.J., "Impact Failure Characteristics in Sandwich Structures: Part II. Effects of Impact Speed and Interfacial Strength," International Journal of Solids and Structures, **39**, *4237–4248 (2002).*

7. Barsoum, R.S., "Application of the Finite Element Iterative Method to the Eigenvalue Problem of a Crack Between Dissimilar Media," International Journal for Numerical Methods in Engineering, **26**, *541–554 (1988).*

8. Rice, J.R., "Elastic Fracture Mechanics Concepts for Interfacial Cracks," Journal of Applied Mechanics, **55**, *98–103 (1988).*

9. Hutchinson, J.W. and Suo, Z., "Mixed Mode Cracking in Layered Materials," Advances in Applied Mechanics, **29**, *63–191 (1992).*

10. Mattheck, C., 1998. Design in Nature: Learning from Trees, Springer-Verlag, New York.

11. Rabin, B.H., Williamson, R.L., Bruck, H.A., Wang, X-L., Watkins, T.R., Feng, Y-Z., and Clarke, D.R., "Residual Strains in an Al203–Ni Joint Bonded With a Composite Interlayer: Experimental Measurements and FEM Analyses," Journal of the American Ceramics Society, **81**, *1541–1549 (1998).*